Volume 3 | Number 6 | November 2018 | Pages 559–650

Nanoscale Horizons

The home for rapid reports of exceptional significance in nanoscience and nanotechnology

rsc.li/nanoscale-horizons

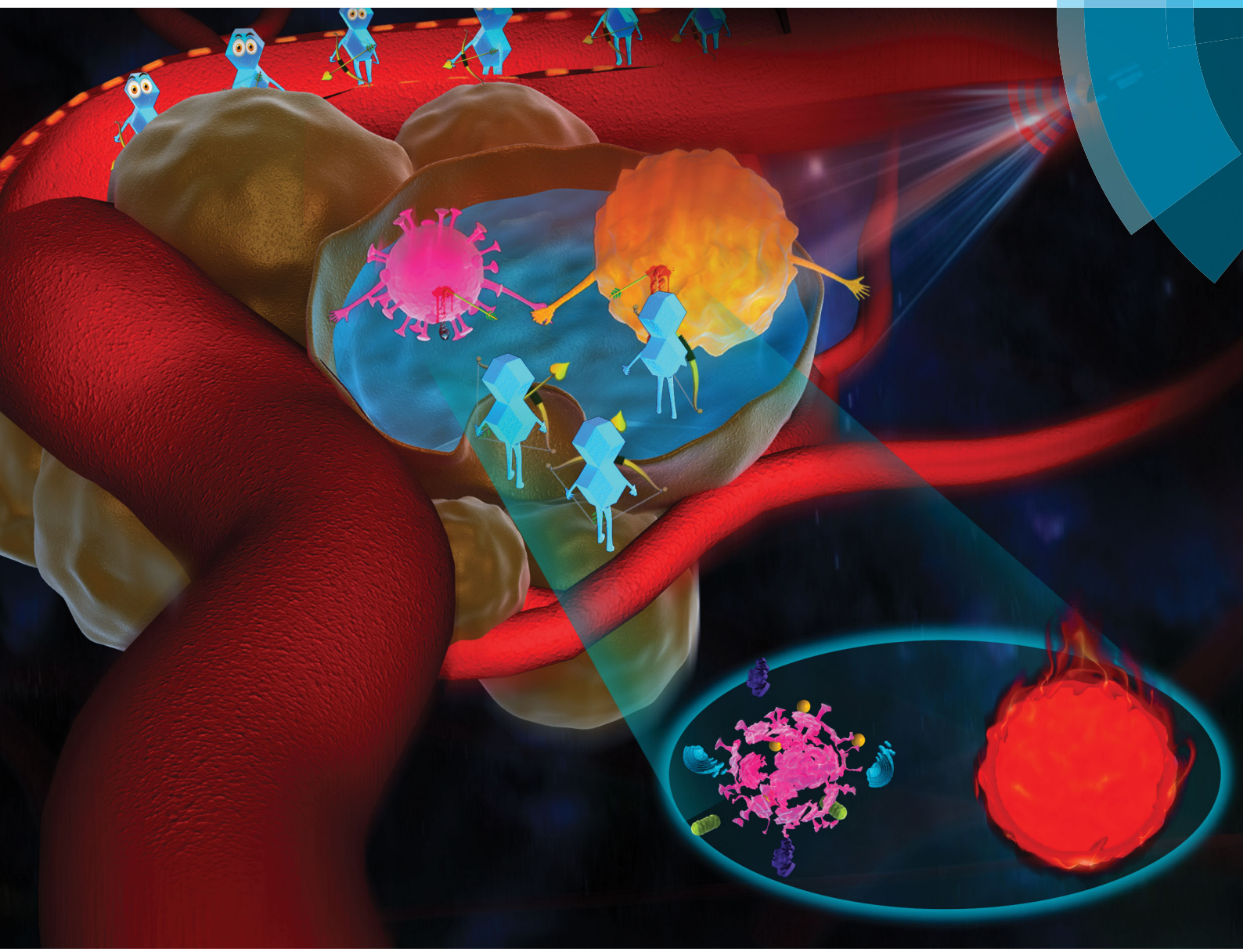

ISSN 2055-6756

ROYAL SOCIETY OF CHEMISTRY

COMMUNICATION

Ping Liang, Yu Zhang, Xianwei Meng *et al.*

A tumor treatment strategy based on biodegradable BSA@ZIF-8 for simultaneously ablating tumors and inhibiting infection

NCNST

Nanoscale Horizons

COMMUNICATION

View Article Online
View Journal | View Issue

Cite this: *Nanoscale Horiz.*, 2018, 3, 606

Received 19th May 2018,
Accepted 3rd July 2018

DOI: 10.1039/c8nh00113h

rsc.li/nanoscale-horizons

A tumor treatment strategy based on biodegradable BSA@ZIF-8 for simultaneously ablating tumors and inhibiting infection†

Qiong Wu,‡[a] Mei Li,‡[b] Longfei Tan,[a] Jie Yu,[c] Zengzhen Chen,[a] Liuhui Su,[a] Xiangling Ren,[a] Changhui Fu,[a] Jun Ren,[a] Laifeng Li,[a] Feng Cao,[d] Ping Liang, *[c] Yu Zhang*[b] and Xianwei Meng *[a]

Studies have shown a clear correlation between cancer incidence and infection, and cancer treatment can also trigger infection so as to lead to an inflammatory response. In this case, we have designed a new tumor treatment strategy based on biodegradable BSA@ZIF-8 for simultaneously ablating tumors and inhibiting infection. This biodegradable ZIF contains abundant porous structures, showing increased absorption of ions and inelastic collisions. A large amount of frictional heat produced by the collisions results in increased tumor cell death under microwave irradiation. This can effectively inhibit tumor growth in mice by microwave ablation with a good anti-tumor effect (95.4%). Intriguingly, the Zn^{2+} released from the degradation of BSA@ZIF-8 causes damage to bacterial cell walls, and destruction of the metabolism and structure of the membrane, leading to bacterial cell death, and ultimately achieving good anti-bacterial properties. Moreover, BSA@ZIF-8 is biodegradable without long-term toxicity *in vivo*. The *in vivo* experimental results show that BSA@ZIF-8 can protect 80% of the mice from lethal challenge with tumors and the accompanying infection. Overall, we present a novel strategy using biodegradable ZIFs for microwave ablation therapy with simultaneous antibacterial and anti-infection effects for the first time, which has achieved good tumor treatment outcomes.

Conceptual insights

The proof-of-concept strategy based on biodegradable BSA@ZIF-8 for simultaneously ablating tumors and inhibiting infection has achieved good therapeutic effects towards tumors. The combination of tumor eradication and infection inhibition can overcome the limitation of microwave ablation, solve the bacterial infection caused by clinical microwave ablation, and improve the curative effects of tumor treatment. However, this effective anti-tumor strategy is still in its infancy. In this case, the strategy of using microwave ablation to treat tumors and simultaneously prevent infection can overcome the current concerns of effective cancer treatment, open a new door for the treatment of tumors, and hopefully encourage researchers to develop more new tumor treatment strategies.

Introduction

Malignant tumors are one of the most serious threats to human health and life, whose incidence is increasing worldwide.[1–3] The treatments for cancer have been well developed in recent years.[4–10] Among the treatments, tumor thermal therapy has been extensively explored, which is referred to as the fifth type of cancer treatment except surgery, chemotherapy, radiotherapy and biotherapy.[11–13] Tumor thermal therapy can either directly kill cancer cells or be used as an auxiliary treatment for improving the sensitivity of radiotherapy and chemotherapy.[14–16] Photothermal therapy is the most widely researched thermal therapeutic method.[17–19] A lot of photothermal agents have been developed for ablating tumors by converting optical energy into heat. However, photothermal therapy is only suitable for the treatment of superficial tumors due to the shallow penetration depth of the laser, which limits the development of its clinical direction,[20–22] while microwave thermal therapy can solve this problem and shows good application prospects.[23–25] It has many advantages such as being minimally invasive, long penetration depth, local controllability, high heating efficiency and large range of ablation.[26–28] Microwave-sensitive materials have been developed very well for enhanced tumor microwave ablation; however, eradication of tumors by this method is still unable to achieve the curing of tumors in the clinic or in practice. This is likely to be caused by the complexity of cancer.

It is demonstrated that infection is one of the most important aspects of tumor complexity. Over the past few decades, studies have shown a clear correlation between cancer incidence and infection. According to several epidemiological and related studies, the occurrence and development of various tumors are

[a] *Laboratory of Controllable Preparation and Application of Nanomaterials, Key Laboratory of Cryogenics, Technical Institute of Physics and Chemistry, Chinese Academy of Sciences, No. 29 East Road Zhongguancun, Beijing 100190, P. R. China*
[b] *Department of Orthopedics, Guangdong General Hospital, Guangdong Academy of Medical Sciences, Guangzhou 510080, China*
[c] *Department of Interventional Ultrasound, Chinese PLA General Hospital, Beijing 100853, P. R. China*
[d] *Department of Cardiology, Chinese PLA General Hospital, Beijing 100853, P. R. China*

† Electronic supplementary information (ESI) available. See DOI: 10.1039/c8nh00113h

‡ These authors contributed equally to this work.

related to infection.[29] For example, gastric cancer is associated with *Helicobacter pylori* infection. The infection plays an important role in the proliferation, survival and metastasis of tumor cells.[30,31] Some researchers also found that the incidence of tumors decreased when the intensity of the inflammatory response caused by infection was reduced.[32] Tumor cells themselves can also secrete various active substances, such as CSF-1 and COS-2, further aggravating the inflammatory response and forming a vicious cycle.[33]

In addition, cancer treatment can also trigger an infection that leads to an inflammatory response, trauma, tissue damage, and stimulation of tumor regeneration and treatment resistance.[34,35] There are also infections in the treatment of clinical oncology, among which a bone tumor is the most serious after bacterial infection, and the mortality rate is almost 100%. Thermal therapy, as an effective treatment for cancer, also triggers an infection inevitably.[36,37] In turn, an infection further stimulates the regeneration of tumors and hinders the subsequent treatment. These results further verify the association between tumors and infection and the difficulty of the resulting tumor therapy. Therefore, a combination of tumor eradication and infection inhibition may overcome the limitations of MW ablation and achieve an enhanced anti-tumor efficacy; however, the research of such an effective anti-tumor strategy is still nascent.

Metal–organic frameworks (MOFs) are a promising option for this feature because most of the metal ions that make up their periodic reticular structures have antibacterial properties.[38,39] MOFs are widely used in many applications, including catalysis, gas separation and storage, and drug delivery, due to their large surface area, adjustable pore size, diversified structure, and good biodegradability.[40–42] As a subclass of MOFs, zeolitic imidazolate frameworks (ZIFs) have also made a major breakthrough in research, especially in drug delivery for tumor therapy. For example, ZIFs were used as pH-sensitive drug delivery vehicles for the enhanced delivery of anticancer 5-FU, doxorubicin (DOX), and CpG oligodeoxynucleotides (ODNs).[43–45]

Herein, we have designed a new therapeutic strategy based on biodegradable BSA@ZIF-8, which can treat tumors by microwave ablation and simultaneously inhibit the growth of bacteria and resist the infection associated with tumor therapy. ZIFs were synthesized through a facile, mild one-pot method. With the coating of bovine serum protein (BSA), long circulation was realized, which showed great prospects in the treatment of tumors. The as-prepared BSA@ZIF-8 exhibited a favorable microwave heating effect *in vitro* due to the large surface area and porous structure, which can absorb a large number of ions in the cavities. In the meantime, Zn^{2+} produced from BSA@ZIF-8 degradation enabled it to exhibit strong antibacterial properties, so that it can be used as an antibacterial agent to inhibit bacterial infection. The as-prepared BSA@ZIF-8 was used in dual treatment for the first time to eradicate tumors and inhibit infection. The *in vivo* anti-tumour and anti-infection effects accompanied by microwave ablation therapy were studied with mice bearing H22 tumors and MRSA infection. The tumor treatment by microwave ablation has good anti-tumor effects (95.4%) in the mice. At the same time, it can also inhibit the bacterial growth and resist the infection associated with tumor therapy. At 8 days after treatment, the number of white blood cells, which reflects inflammation in the treatment group with ZIFs, had been restored, while the treatment group without ZIFs was still 50% higher than the initial value on day 14. This strategy has succeeded in achieving tumor therapy through tumor microwave ablation therapy while simultaneously inhibiting infection. The biodegradable BSA@ZIF-8 can be a powerful tool to improve microwave ablation therapy by simultaneously ablating tumor tissue and resisting infection.

Results and discussion

Synthesis and characterization

In this study, a simple method was used to successfully synthesize BSA@ZIF-8, which was well characterized by TEM images and SEM images (Fig. 1 and Fig. S1, ESI†). BSA@ZIF-8 was obtained from ZIF-8 by surface coating BSA. ZIF-8 was synthesized first by its self-assembly and then coated with protein to improve its biocompatibility. The obvious cube structure can be seen in the as-synthesized ZIF-8 under TEM, which had sharp edges and corners. After the BSA coating, a layer of protein can be found on the surface. The average diameter of the monodisperse ZIF-8 was measured to be ≈105 nm, while the resulting BSA@ZIF-8 with a mean diameter of ≈110 nm was prepared (Fig. 1d and h). The hydrodynamic size of ZIF-8 and BSA@ZIF-8 was 139.8 nm and 153.9 nm respectively, which was determined by dynamic light scattering (Fig. S2a and b, ESI†). The dispersion ability of BSA@ZIF-8 in phosphate-buffered saline (PBS) and normal saline (NS) solutions was evaluated and the photographs are shown in Fig. S3 (ESI†). Dynamic Light Scattering (DLS) was also employed to evaluate the stability of BSA@ZIF-8 (Fig. S4, ESI†), and the result showed that BSA@ZIF has certain stability in neutral PBS and NS. The size and dispersibility of the as-prepared BSA@ZIF-8 were suitable for the EPR effect.[46] The TEM-mapping of BSA@ZIF-8 (Fig. S1b–e, ESI†) indicated that the elemental distributions of C, N, O, and Zn were uniform in the structure. Feature elements in BSA@ZIF-8 were confirmed by EDS (Fig. S1f, ESI†), which showed the elemental contents in the structure, and the result was consistent with the elemental mapping. FTIR spectrometry was measured to evaluate the synthesis of BSA@ZIF-8 (Fig. S2c, ESI†). The peaks at 690 cm^{-1} and 3421 cm^{-1} correspond to the plane bending vibration and telescopic vibration of O–H respectively.

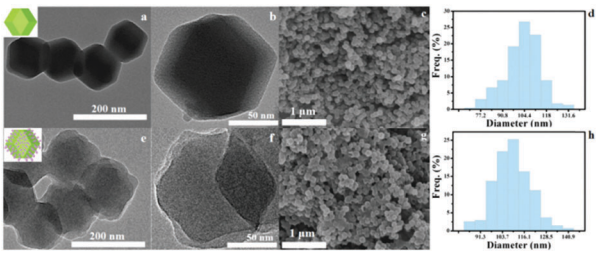

Fig. 1 (a and b) TEM images of ZIF-8 under different amplification multiples. (c) SEM image of ZIF-8. (d) The size obtained through analyzing the SEM image of ZIF-8. (e and f) TEM image of BSA@ZIF-8 under different amplification multiples. (g) SEM image of BSA@ZIF-8. (h) The size obtained through analyzing the SEM image of BSA@ZIF-8.

The peak at 1135 cm^{-1} corresponds to the imidazole skeleton telescopic vibration from ZIF-8, while the peak at 1654 cm^{-1} was the stretching vibration absorption of C=O which was from BSA, confirming the successful synthesis of BSA@ZIF-8.[47,48] The zeta potentials of the as-prepared ZIF-8 and BSA@ZIF-8 were 18.0 and −14.7 mV respectively (Fig. S2d, ESI†), further verifying the successful synthesis of BSA@ZIF-8.

Antibacterial effects of ZIF-8 and BSA@ZIF-8 *in vitro*

In the past few years, MOFs in antibacterial research have made considerable progress. The reason for their antibacterial properties may be that MOFs are unstable in aqueous solution, and the metal ions are released as antibacterial agents.[49–51] As a subclass of MOFs, there were also a few reports about ZIFs for antibacterial applications, but they were used as carriers to load antibacterial agents instead of using the ZIFs themselves.[52,53] To evaluate the antibacterial properties of BSA@ZIF-8, an agarose diffusion assay was conducted first. The results are shown in Fig. 2a and b, and the inhibition zones of ZIF-8 and BSA@ZIF-8 against MRSA and resistant *E. coli* were represented with the antibacterial properties of ZIF-8 and BSA@ZIF-8, respectively. The samples without materials had no signs of inhibition zones. For comparison, there were significant inhibition zones that can be observed around the various concentrations of ZIF-8 and BSA@ZIF-8. The size of the inhibition zone indicated that BSA@ZIF-8 had concentration-dependent antibacterial effects. As the concentration of BSA@ZIF-8 increased, the size of the inhibition zone increased. And when the concentration of BSA@ZIF-8 increased from 3.125 to 100 μg mL^{-1}, the diameters of the inhibition zones against MRSA and resistant *E. coli* were increased from 0 to 12.07 mm and from 0 to 9.4 mm, respectively. However for ZIF-8, the diameters against MRSA and resistant *E. coli* were a little larger; with the concentrations changing from 3.125 to 100 μg mL^{-1}, the diameters increased from 1.12 to 15.86 mm and from 0 to 11.99 mm, respectively. From the characteristics of the inhibition zones, it can be demonstrated that ZIF-8 and BSA@ZIF-8 show good antibacterial activity. The reason for the antibacterial effects of ZIFs may be that the ions produced by ZIF degradation have strong antibacterial properties.[54] The surface of the bacteria was negatively charged due to the presence of free –COOH groups, and the slow release of Zn^{2+} was adsorbed at the surface of the bacteria with coulombic attraction, causing the cell wall of the bacteria to be damaged. After that, Zn^{2+} further penetrated the cell wall, replaced the position of the cations on the cell membrane surface, combined with proteins or other anionic groups, and destroyed the metabolism and structure of the membrane, which made the cell membrane lose its biological function, leading to bacterial cytoplasm outflow, eventually leading to cell death and achieving the goal of antibacterial properties.[55,56] Meanwhile, excess Zn^{2+} penetrated into the interior of the cell membrane of the cell and reacted with the sulfur and nitrogen functional groups of the bacteria, such as the sulphur (–SH) and amino (–NH:) groups of proteins, nucleic acids and so on, so as to cause protein denaturation and loss of cell synthetase activity.[57,58] It also reacted with DNA to disrupt the normal activities of some functional systems (such as respiratory, electron transport, and material transmission) in the cell and interfere with normal metabolic processes.[59] Through the above methods, Zn^{2+} acts on the bacteria, causing the death of the bacteria or the dysfunction of the bacteria, and finally achieves the antibacterial properties. But when the bacteria were killed, it dissociated from the bacteria and then contacted with other bacteria, repeating the antibacterial activity and showing excellent antibacterial properties.[60] What's more, the results showed that the antibacterial effects of ZIF-8 and BSA@ZIF-8 on MRSA were better than those of the resistant *E. coli*. This phenomenon can be attributed to the difference in the groups and structures on the surface of the bacteria.[61]

To further test the antibacterial properties of BSA@ZIF-8, the minimal inhibition concentration was determined, and the results were consistent with the agarose diffusion assay. As shown in Fig. 2c, the minimal inhibition concentrations of BSA@ZIF-8 on MRSA and resistant *E. coli* were 25 and 50 μg mL^{-1}, respectively, while the minimal inhibition concentrations of ZIF-8 on MRSA and resistant *E. coli* were slightly lower than those of BSA@ZIF-8, which were 6.25 and 12.5 μg mL^{-1} respectively. The above results further verified that ZIF-8 and BSA@ZIF-8 had good antibacterial activity. Fig. 2d and e show the MRSA cell SEM images of the negative control and the BSA@ZIF-8, respectively.

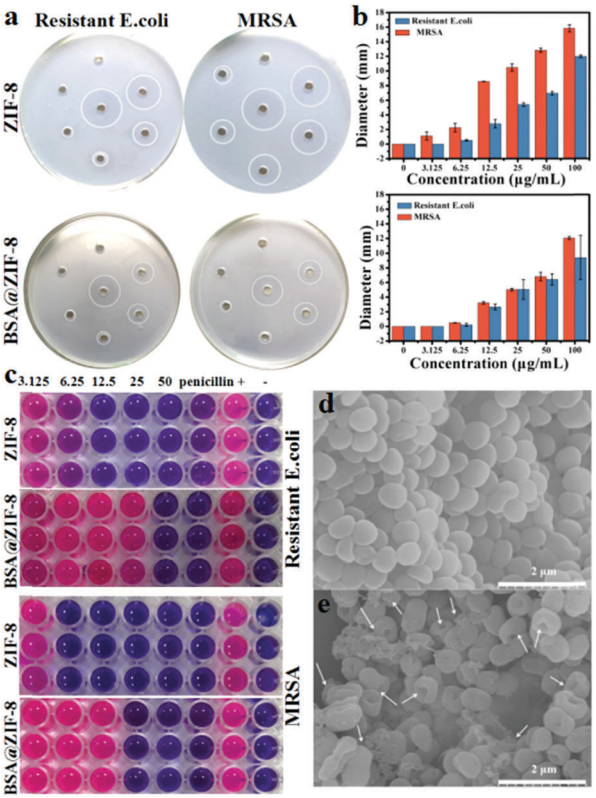

Fig. 2 (a) The inhibition zones of ZIF-8 and BSA@ZIF-8 against MRSA and resistant *E. coli* through agarose diffusion assays. (b) The diameter of the inhibition zone based on (a). (c) The minimal inhibition concentrations of ZIF-8 and BSA@ZIF-8 on MRSA and resistant *E. coli*. (d) SEM image of normal MRSA. (e) SEM image of MRSA which was treated with BSA@ZIF-8 for 6 h; the arrows indicated perforation and cytoplasmic leakage.

The SEM images also showed that BSA@ZIF-8 induced strong damage against the bacterial membrane, which was reflected in a large number of membrane perforations and extensive cytoplasmic leakage (Fig. 2d), while that of the control group was smooth and well shaped (Fig. 2e). Therefore, it can be concluded that BSA@ZIF-8 has remarkable antibacterial effects *in vitro*.

Microwave heating properties of ZIF-8 and BSA@ZIF-8 *in vitro*

In our previous studies, great efforts have been made to design microwave-sensitive agents which increased the tumor temperature for tumor microwave ablation therapy.[23–26] Meanwhile, the microwave heating principle of microwave-sensitive agents was also explored. For example, due to the sensitivity of ionic liquids to microwaves in an enclosed space, a microwave-sensitive agent was designed by encapsulating ionic liquids in hollow nanospheres.[62,63] However in this work, ZIF-8 showed excellent microwave heating characteristics without encapsulating any microwave sensitizers. It is well known that the heating of microwave irradiation is caused by the frictional heat of removable water or ions. Therefore, whether water or ions were more conducive to promoting the microwave heating effect of ZIF-8 was studied. As shown in Fig. S5 (ESI†), there was no obvious temperature change in water or in the aqueous solution of ZIF-8 after 5 min at 1.8 W and 450 MHz microwave irradiation, while the temperature of the saline solution was increased to 39.7 °C. In addition, the temperature of the saline solution containing ZIF-8 increased more significantly (Fig. S6, ESI†), indicating that the ions play an important role in the heating of microwave irradiation. Furthermore, it was found that the material itself has good microwave heating effects and concentration dependence. When the concentration of ZIF-8 was 1, 2, and 10 mg mL^{-1}, the temperature increased to 21.4, 24.8, and 29.5 °C respectively after 5 min at 1.8 W and 450 MHz microwave irradiation (Fig. 3a and b). However the temperature change in the control group was only 15.3 °C. This indicates that the temperature changes in the experimental groups were respectively 6.1, 9.5, and 14.2 °C higher than those in the control group, which proved that ZIF-8 itself has good microwave heating effects and concentration dependence. The results indicated that ZIF-8 is more conducive to converting microwave energy into thermal energy due to the confinement effect of the porous structures.[64] The results of N_2 isothermal adsorption–desorption indicated that the specific surface area of ZIF-8 was 1299.82 $m^2\ g^{-1}$ (Fig. S7a, ESI†), and the average micropore diameter of it was about 8.0 Å (Fig. S7b, ESI†). Because ZIF-8 has a large surface area and porous structure, it can absorb a large number of ions in such a closed area. Under microwave irradiation, a powerful inelastic collision of ions and ZIF-8 was produced, resulting in a large amount of frictional heat. However for the saline solution without ZIF-8, the frequency of collision between the ions was low in free space, resulting in less frictional heat. Therefore, ZIF-8 had excellent microwave heating effects under microwave irradiation, which can be used as a microwave sensitizer.

As for BSA@ZIF-8, the microwave heating effect was also evaluated. After microwave irradiation for 5 min, the temperature changes were respectively 19.2, 21.5, and 26.1 °C for 1, 2, and 10 mg mL^{-1} BSA@ZIF-8 (Fig. 3c and d). The temperature change in the control group was 15.1 °C, which indicates that the temperature changes in BSA@ZIF-8 were respectively 4.1, 6.4, and 11 °C higher than those in the control group. Similarly, BSA@ZIF-8 has good microwave heating effects and concentration dependence. In addition, the microwave heating experiments of ZIF-8 and BSA@ZIF-8 were also carried out simultaneously for comparison. The temperature of ZIF-8 and BSA@ZIF-8 saline solution (10 mg mL^{-1}) increased by 29.6 and 26.6 °C respectively after microwave irradiation for 5 min (Fig. 3f). The temperature of the control saline solution was increased from 28.1 to 43.5 °C, which indicates that the temperature increased by 15.4 °C. The temperature changes in the solutions were recorded by a FLIR imaging instrument every minute, and the results are shown in Fig. 3e. The results demonstrated that ZIF-8 and BSA@ZIF-8 had excellent microwave heating effects under microwave irradiation. The microwave thermal efficiency of BSA@ZIF-8 was calculated to be 26.86% at 10 mg mL^{-1} in saline solution (Fig. S4, ESI†),[64] which was at a high thermal conversion efficiency level compared to previously reported microwave sensitizers.[62,63] All of the above results indicate that ZIF-8 and BSA@ZIF-8 were suitable for tumor microwave thermal therapy *in vivo*.

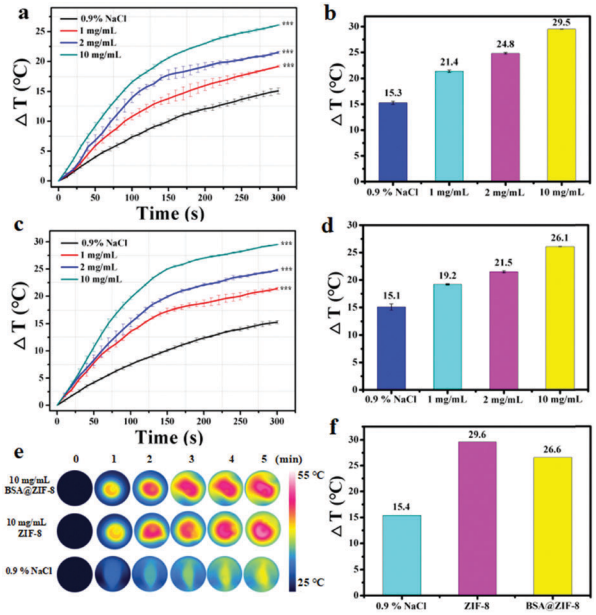

Fig. 3 (a) The heating curves of ZIF-8 *in vitro* at different concentrations (0, 1, 2, and 10 mg mL^{-1}, saline water was used as the control). (b) Temperature change values at different concentrations based on (a). (c) The heating curves of BSA@ZIF-8 *in vitro* at different concentrations (0, 1, 2, and 10 mg mL^{-1}, saline water was used as the control). (d) Temperature change values at different concentrations based on (c). (e) FLIR images of the control, ZIF-8 and BSA@ZIF-8 at every minute. (f) Temperature change values of different materials.

Evaluation of biocompatibility *in vitro* and *in vivo*

In view of the favourable microwave heating effects and antibacterial effects of ZIF-8 and BSA@ZIF-8 *in vitro*, they were expected to have good microwave heating effects and remarkable antibacterial effects *in vivo*. Therefore, the cytotoxicity and

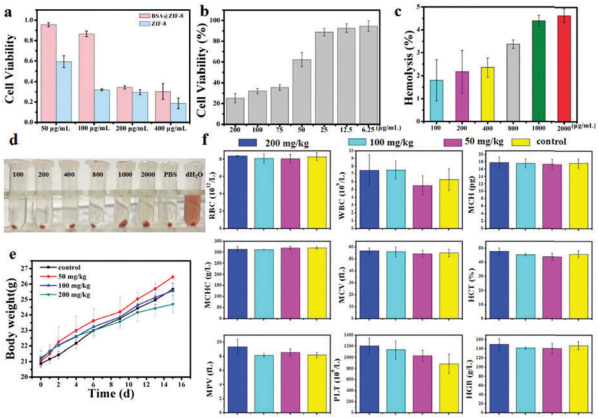

Fig. 4 (a) The cytotoxicity of ZIF-8 and BSA@ZIF-8 at different concentrations. (b) The cytotoxicity of ZIF-8 at different concentrations. (c) The hemolysis rate of BSA@ZIF-8 at different concentrations. (d) The hemolytic study of BSA@ZIF-8 at different concentrations. (e) Body weight changes of BSA@ZIF-8 in acute toxicity experiments at different doses (0, 50, 100, and 200 mg kg^{-1}). (f) Blood routine examination including RBC, WBC, MCH, MCHC, MCV, HCT, MPV, PLT, and HGB of each group for BSA@ZIF-8 (0, 50, 100, and 200 mg kg^{-1}) *via* tail vein injection *in vivo*.

biocompatibility should be taken into consideration. The cytotoxicity of ZIF-8 and BSA@ZIF-8 was evaluated by an MTT experiment first. As shown in Fig. 4a, the viability of cells treated with BSA@ZIF-8 was more than 80% even at a high concentration of 100 μg mL^{-1}, indicating the low cytotoxicity of BSA@ZIF-8. However ZIF-8 had very high cytotoxicity, as even at a low concentration of 50 μg mL^{-1}, the viability of the cells was only 60%. When the concentration was lower than 25 μg mL^{-1}, the cell viability of ZIF-8 was higher than 80% (Fig. 4b). This indicates that the cytotoxicity of BSA@ZIF-8 was significantly reduced after the BSA modification, which could be used *in vivo*, while ZIF-8 was difficult to use *in vivo* due to its high toxicity. Next, a hemolysis test was also performed on the as-prepared BSA@ZIF-8 at different concentrations to evaluate the biocompatibility. The results showed that there was no obvious hemolysis (Fig. 4c and d). The hemolysis rate was less than 5% even at the highest concentration of 2000 μg mL^{-1}, indicating the good biocompatibility of BSA@ZIF-8.

To further explore the biocompatibility of the as-prepared BSA@ZIF-8 *in vivo*, an acute toxicity experiment was performed. BSA@ZIF-8 was injected into the mice *via* tail vein injection at different doses (50, 100, and 200 mg kg^{-1}). Then, the body weights of the mice were recorded in detail and are shown in Fig. 4e, showing no significant toxicity even at a high dose of 200 mg kg^{-1}. The mice were sacrificed 2 weeks post-injection, and then the blood and the major organs of the mice were collected for further pathological analysis. The indexes of the blood routine examination are shown in Fig. 4f, including red blood cells (RBCs), white blood cells (WBCs), mean capacity hemoglobin (MCH), mean corpuscular hemoglobin concentration (MCHC), mean corpuscular volume (MCV), hematocrit (HCT), mean platelet volume (MPV), platelets (PLTs), and hemoglobin (HGB). Compared with the control group, none of the groups in this experiment showed significant differences. The blood biochemical analysis is shown in Fig. S8 (ESI†), including aspartate aminotransferase (AST), alanine aminotransferase (ALT), creatinine (CREA), and urea (UREA). No significant liver damage or renal impairment was found. Representative histological images of the main organs (heart, liver, spleen, lung, and kidney) of each experimental group are shown in Fig. S9 (ESI†), indicating no obvious damage or inflammation lesions when compared with the control group. These results demonstrated that the toxicity of BSA@ZIF-8 was low enough and deserved further study *in vivo*.

Anti-tumour and anti-infection effects *in vivo*

Inspired by its ideal microwave heating effect, remarkable antibacterial effect and favorable biocompatibility, the as-prepared BSA@ZIF-8 was expected to be used in further animal experiments. Microwave ablation therapy, a minimally invasive tumor therapy, which is targeted and localized in the tumor site, causes irreversible tumor cell damage and necrosis, achieving a longer survival period.[23–25] To evaluate the microwave heating effect and antibacterial effect of the as-prepared BSA@ZIF-8 on subcutaneous tumors, microwave irradiation and MRSA infection were applied to the mice for tumor microwave ablation and anti-infection due to the connection between cancer and infection.[65]

A tumor-targeting study was conducted on the distribution of BSA@ZIF-8 in the mice first to find the best treatment time. The content of BSA@ZIF-8 in each organ was detected by ICP-MS (Fig. S10, ESI†). The results showed that after injection the content of BSA@ZIF-8 in the tumor was the highest at 6 h (8.21%), higher than that at 4 h (6.35%), 8 h (6.40%), and 24 h (3.70%). Therefore, microwave irradiation was performed on the tumor site of the mice 6 h post-injection *via* tail vein injection in the anti-tumor experiment. Then MRSA infection was conducted through puncturing the skin of the tumor area with a sterile syringe and coating with an MRSA strain. During the microwave irradiation, the temperature at the tumor site was monitored by a FLIR imaging instrument in real time. As shown in Fig. 5a and b, with the increase of microwave irradiation time, the temperature of the tumor area continued to increase, and the central hot zone gradually diffused around. It can be seen from the figure that the microwave heating effect of the BSA@ZIF-8 + MW + infection group was more obvious *in vivo* than that of the MW + infection group. The final temperatures of both microwave groups rapidly increase to more than 55 °C, which was higher than the critical temperature of the tumor ablation needed (> 42 °C).[12,66] The temperature change in the BSA@ZIF-8 + MW + infection group was 35.03 ± 1.57 °C, while that of the MW + infection group was 24.53 ± 0.77 °C. Therefore, the rapid microwave heating effect of the as-prepared BSA@ZIF-8 *in vivo* was significant for tumor ablation therapy.

Considering the complexity of the tumor and the increasing evidence of its association with infection,[65] our treatment strategy required simultaneous infection resistance and tumor microwave ablation. At the same time as tumor microwave ablation, the antibacterial properties of BSA@ZIF-8 were also

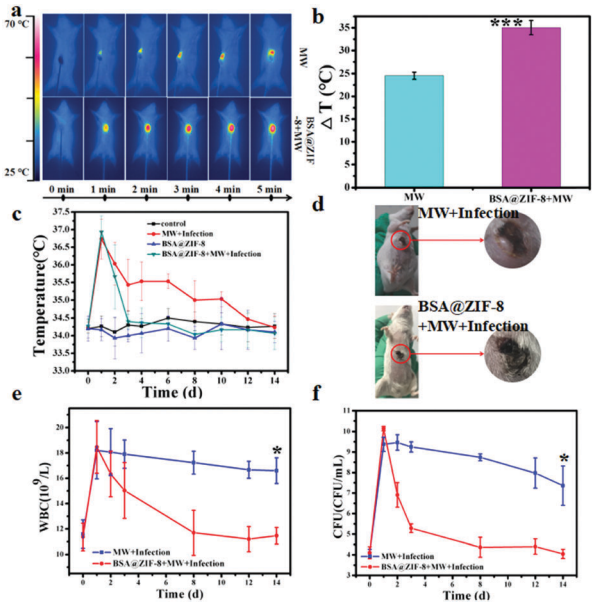

Fig. 5 (a) FLIR images of the mice in the microwave and BSA@ZIF-8 + MW groups at 1 min intervals. (b) Temperature change values in the microwave and BSA@ZIF-8 + MW groups. (c) Tumor temperature change curves in all experimental groups for 14 days. (d) The photos of the mice on the first day after treatment of simultaneous microwave ablation and infection in the MW + infection group and the BSA@ZIF-8 + MW + infection group. (e) The number of WBCs in the MW + infection group and the BSA@ZIF-8 + MW + infection group for 14 days. (f) The number of bacterial colonies in the tumor area of the MW + infection group and the BSA@ZIF-8 + MW + infection group for 14 days.

investigated *in vivo*. After tumor microwave ablation, MRSA infection was performed on the tumor site near the wound, and then the daily tumor temperature of the infected mice was recorded and is shown in Fig. 5c. The tumor temperatures of the infected mice were raised after the MRSA infection. At the first day after the treatment, the tumor temperatures of the BSA@ZIF-8 + MW + infection group and the MW + infection group increased up to 2.67 and 2.50 °C respectively compared with the day before being infected. A photo of the mice was also taken on the first day after treatment in the MW + infection group and the BSA@ZIF-8 + MW + infection group (Fig. 5d). It can be intuitively seen that the mice in both groups had clear puncture marks and even festering, which confirmed the successful MRSA infection and inflammatory responses. As time went on, the tumor temperatures began to decline. And by the 3rd day, the tumor temperature in the BSA@ZIF-8 + MW + infection group returned to normal while that of the MW + infection group had only begun to approach the normal level by the 12th day. But the tumor temperatures had little change in the control group and the BSA@ZIF-8 group, and the change values were within 0.5 °C. These results indicated that MRSA infection successfully caused local skin infections and subsequently produced an inflammatory response, leading to increased tumor temperatures in the mice. The amount of white blood cells (WBCs) was also analyzed and is shown in Fig. 5e. At the first day after the treatment, the amount of WBCs increased to 6.6×10^9 L^{-1} and 7.1×10^9 L^{-1} respectively in the MW + infection group and the BSA@ZIF-8 + MW + infection group, both higher than the normal level, and then gradually decreased every day. When it came to the 8th day, the amount of WBCs was already at the normal level in the BSA@ZIF-8 + MW + infection group while that of the MW + infection group was higher than the normal level for 14 days although it has been falling over time. The result was consistent with the changes in tumor temperature, as shown in Fig. 5c. The number of bacterial colonies in the tumor area was also counted through the flat colony counting method. As shown in Fig. 5f, the number of bacterial colonies in the both groups on the first day after the treatment was more than doubled before the infection and then began to decline. The corresponding spread plate pictures are shown in Fig. S11 (ESI†). The number of bacterial colonies in the MW + infection group decreased slowly, and ultimately was 80% higher than the number before the infection, while that of the BSA@ZIF-8 + MW + infection group ended up with the same number as pre-infection. This was consistent with the changes in the amount of WBCs, indicating successful infection and inhibition. All of the above results, namely the temperature of the tumor sites, the number of WBCs, and the number of bacterial colonies showed that BSA@ZIF-8 effectively inhibited the development of infection in the treated mice. Therefore, BSA@ZIF-8 can inhibit bacterial growth *in vivo* and manage the infection, which accompanies tumor microwave ablation therapy.

After the treatment, there were still residual tumors in the MW + infection group and the tumor volume increased gradually over time, while it was completely ablated in the BSA@ZIF-8 + MW + infection group by microwave ablation therapy. On the 4th day after treatment, a mouse in the BSA@ZIF-8 + MW + infection group had tumor recurrence. The tumor volume in each group for 14 days was measured and is shown in Fig. 6a. After 14 days of treatment, the tumor volume of the BSA@ZIF-8 + MW + infection group was the smallest, which expressed a more significant microwave ablation therapy effect in the tumor than

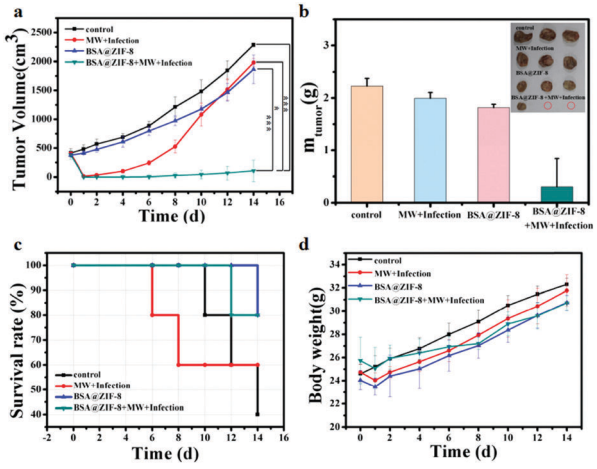

Fig. 6 (a) Tumor volume growth curve of different groups for 14 days. (b) The tumor weight in different groups 14 days after treatment; the inset photo is the extracted tumors. (c) Survival rate curves of different groups for 14 days. (d) Body weight changes of different groups for 14 days.

the other groups. This also showed that although the temperature of the tumor central site was higher than that of tumor cell necrosis and ablation, it was still not enough to kill the surrounding tumor cells completely. The tumor inhibition rate was calculated. The tumor inhibition rate of BSA@ZIF-8 + MW + infection was 95.37%, far higher than that of the BSA@ZIF-8 group (18.42%) and the MW + infection group (13.30%). The weight of the extracted tumor after being treated for 14 days is shown in Fig. 6b, and the photo of the extracted tumors also obviously showed the therapeutic effect that the tumor in the BSA@ZIF-8 + MW + infection group was far smaller than that of the other groups, and the tumors of 3 mice disappeared. The control group and the MW + infection group were left with only 3 mice and 2 mice at the end of the experiment. The results indicated that BSA@ZIF-8 had effective tumor therapy outcomes due to its enhanced microwave ablation and remarkable antibacterial properties.

The survival rates of the BSA@ZIF-8 + MW + infection, BSA@ZIF-8, MW + infection, and control groups were 80%, 80%, 60%, and 40% respectively after being treated for 14 days (Fig. 6c). The deaths of mice in the MW + infection group were first observed on day 6 after treatment, and the deaths in the control, BSA@ZIF-8, and BSA@ZIF-8 + MW + infection groups appeared on the 10th, 12th, and 10th day, respectively. It was demonstrated that BSA@ZIF-8 could protect 80% of the mice from death due to the tumor and its accompanied infection. The weight of the mice is shown in Fig. 6d. In addition to the mice in the control group, the weight of the other mice decreased at varying degrees on the first day after being treated, and then began to increase over time. During the treatment days, no signs of body weight loss and acute toxicity were observed. In combination with the representative histological images (Fig. S12, ESI†), it is further suggested that BSA@ZIF-8 was not toxic *in vivo*. Therefore, it can be concluded that BSA@ZIF-8 has favorable microwave ablation therapy effects and significant antibacterial effects, which can be used to treat tumors with microwave ablation while simultaneously inhibiting bacterial infection.

Experimental section

Materials

Sodium chloride (NaCl), anhydrous methanol, and anhydrous ethanol were purchased from the Beijing Chemical Reagents Company (China). Zinc nitrate ($Zn(NO_3)_2{\cdot}6H_2O$) was supplied by Tianjin Chemical Reagent 3 Plant. 2-Methylimidazolate (2MI) was purchased from Beijing Bailingwei Technology Co., Ltd. Bovine serum protein (BSA) was obtained from the Beijing Lanyi Reagents Company (China). The reagents used in this work were of analytical grade (A.R.) without any further purification.

Preparation of BSA@ZIF-8

The method to synthesize ZIF-8 that we used was a facile mild one-pot method. First, $Zn(NO_3)_2{\cdot}6H_2O$ and 2MI were dissolved in methanol respectively. Then, the 2MI methanol solution was added to the $Zn(NO_3)_2{\cdot}6H_2O$ methanol solution, and stirred for 24 hours at room temperature. Then centrifugal separation was performed, and the solid sediment ZIF-8 was obtained, which was washed three times with ethanol and deionized water respectively. The obtained ZIF-8 continued to react, mixing it with BSA in a mixture of aqueous solutions and kept in an ice bath under sonication for 30 min. In this manner, the composite BSA@ZIF-8 was successfully obtained after washing three times with deionized water.

Characterization of the nanoparticles

Transmission electron microscopy (TEM, HT7700, Hitachi, Japan) and scanning electron microscopy (SEM, Models 4300, Hitachi, Japan) were adopted to characterize the size and morphology of the obtained ZIF-8 and BSA@ZIF-8. A high-resolution transmission electron microscope (TEM, JEM-2100, Hitachi, Japan) was employed to characterize the BSA@ZIF-8 morphology and analyze the bulk distribution of C, N, O, and Zn. A zeta-sizer (Malvern Instruments Zeta-sizer Nano ZS90, Britain) was employed to measure the hydrodynamic particle size distribution and zeta-potential. Fourier transform infrared spectrometry (FTIR, Excalibur 3100, Varian, US) was performed to characterize the functional groups of the as-prepared BSA@ZIF-8. Optical micro-confocal fluorescence microscopy (Olympus X71, Japan) was used to observe the tissue sections and cells. A forward-looking infrared (FLIR) imaging instrument was employed to monitor temperature in real time.

Microwave heating effects of BSA@ZIF-8 *in vitro*

The microwave heating effect of BSA@ZIF-8 was evaluated in saline solution (0.9% NaCl) at different concentrations (1, 2, and 10 mg mL^{-1}) under microwave irradiation (1.8 W, 450 MHz) for 5 min in an *in vitro* experiment. The saline solution was used as a control. The temperature change of the solution was collected by a FLIR imaging instrument. The temperature change values were calculated and the temperature change value curves over time were plotted to evaluate the microwave heating properties.

Typical bacterial culture

The antibacterial effect of ZIF-8 and BSA@ZIF-8 were evaluated with the Gram-negative methicillin-resistant *Staphylococcus aureus* (MRSA) and Gram-positive resistant *E. coli*. All items used in the experiment were sterilized by an autoclave prior to use. Luria Bertani (LB) broth and nutrient agar were used as a nutrient source. The bacterial count was measured at 600 nm using optical density (OD). The ideal bacterial density of the antibacterial test was 0.8–1.0 OD concentration, and the ideal concentration of the bacterial suspension was about 10^5 CFU mL^{-1}.

Agarose diffusion assay of ZIF-8 and BSA@ZIF-8

The antibacterial effects of ZIF-8 and BSA@ZIF-8 were evaluated by the experiments of inhibitory zone tests. First, MRSA and resistant *E. coli* were put into LB broth and incubated to an ideal concentration. The process continued for 12 h at 37 °C upon oscillation. After that, the bacterial suspension was diluted to 10^5 CFU mL^{-1}. The pre-prepared nutrient agarose

was added with 1 mL of the bacterial suspension and then poured into Petri dishes. After cooling down, sample holes were punched in the agarose plates. Then, 20 μL of different concentrations of the materials was added into each hole. The Petri dishes continued to be placed on the sterile platform at room temperature for 30 minutes to ensure that the materials in the holes spread to the agarose. After that, the Petri dishes were hatched backwards into the sterile constant temperature incubator overnight at 37 °C. The antibacterial effect was evaluated by the diameter of the clearing area.

Minimum inhibitory concentration test of ZIF-8 and BSA@ZIF-8

The minimum inhibitory concentration test was also investigated on ZIF-8 and BSA@ZIF-8 to evaluate the antibacterial effects. The experiment was performed in a sterile 96-well plate. Six experimental concentrations were set up in the experiment. The control groups were penicillin control, positive control and negative control. There were six parallel groups in each group. The bacterial fluid was added to the sterile 96-well plate first, and then all the materials with different concentrations were added. When everything had been added, the sterile 96-well plate was put into the sterile constant temperature incubator for 16 to 18 h at 37 °C. Then, the resazurin solution (0.0625%) was added into the sterile 96-well plate and continued to incubate in the sterile constant temperature incubator for 4 h. After the incubation was completed, the antibacterial effect was evaluated by the color changes.

Cytotoxic experiments of BSA@ZIF-8

The cytotoxic experiments were investigated through an MTT (methyl thiazolyl tetrazolium) assay. The HepG2 cells were incubated with ZIF-8 and BSA@ZIF-8 at different concentrations (50, 100, 200, and 400 μg mL^{-1}) for 24 h in 96-well plates, then MTT solution (0.5 mg mL^{-1}) was added and continued to incubate. After 4 h, the MTT solution was removed and replaced with 150 μL of dimethyl sulfoxide (DMSO), and then the absorbance was measured at 490 nm. The group that did not have the material added was treated as a control. There were six parallel samples in each group.

Hemolysis assay of BSA@ZIF-8

The blood biocompatibility of BSA@ZIF-8 was also investigated through the red blood cells (RBCs) which were extracted from a rabbit. The RBCs were stabilized by ethylene diamine tetraacetic acid and diluted with PBS. Then, 0.5 mL of the RBCs was added to 0.5 mL of PBS solution containing different concentrations of BSA@ZIF-8 (from 0 to 4000 μg mL^{-1}). The deionized water and PBS were used as the positive control and the negative control respectively. The mixtures were kept static for 3 hours at room temperature and centrifuged at 9000 rpm for 5 min. 100 μL of the supernatant was removed and added into a 96-well plate. Then the absorption peak at 570 nm was measured with UV-Vis spectroscopy.

Acute toxicity experiment of BSA@ZIF-8

Balb/c mice of 22 ± 2 g were divided into four groups (control group, 50 mg kg^{-1}, 100 mg kg^{-1}, and 200 mg kg^{-1}) randomly. Then BSA@ZIF-8 was injected into the mice *via* tail vein injection. The mice were continuously observed for 14 days. And after 14 days, the blood routine analysis and histology study were performed.

Zn content analysis per organ

The content of Zn per organ after intravenous injection of BSA@ZIF-8 (50 mg kg^{-1}) at different times (0, 4, 6, 8, and 24 h) was studied with H22-tumor-bearing mice. The mice were injected with BSA@ZIF-8 (50 mg kg^{-1}) and then sacrificed at different times (0, 4, 6, 8, and 24 h), and the major organs (included tumors, heart, liver, spleen, kidney, and lung) were treated for the ICP-MS experiment.

Anti-tumour and anti-infection assay of BSA@ZIF-8 *in vivo*

The anti-tumour and anti-infection effects of BSA@ZIF-8 *in vivo* were evaluated in H22-tumor-bearing mice. The tumor-bearing mice of 25 ± 1 g were randomly divided into four groups (5 mice in each group with a tumor volume of 400 ± 30 mm^3) in the experiments. The four groups were the control group, the MW + infection group, the BSA@ZIF-8 group, and the BSA@ZIF-8 + MW + infection group. BSA@ZIF-8 was injected with an intravenous dose of 50 mg kg^{-1}. The mice in the microwave irradiated groups were irradiated (1.8 W, 450 MHz) 6 h post-injection for 5 min in the tumor area. After microwave irradiation, the tumor area of the mice was punctured by a sterile syringe needle and infected with 100 μL MRSA fluid whose concentration was 5×10^7 CFU mL^{-1}. During infection and treatment, the mice were examined daily, and the body weight, tumor volume measurement, temperature monitoring, bacterial culture, and leukocyte detection were performed on the infected mice at 24 h, 2 days, 3 days, 8 days and the last day after infection.

Histology study of the acute toxicity experiment and *in vivo* treatment experiment

Histology study of the major organs (heart, liver, spleen, lung, and kidney) was carried out. The extracted tissues were fixed with formalin solution (10%) and embedded in paraffin. Then, the paraffin with the organs was cut into thin slices and stained with hematoxylin and eosin (H&E). Then, an optical microscope (Olympus X71, Japan) was used to judge if there was tissue damage.

Statistical analysis

All of the results were expressed as the mean ± standard deviation (S.D.). The statistical significance of all experiments was $p < 0.05$.

Conclusions

In conclusion, we have successfully developed a new therapeutic strategy based on biodegradable BSA@ZIF-8 for the first time, which can eradicate tumors with enhanced microwave ablation and simultaneously resist infection that is associated with tumor

therapy. These biodegradable ZIFs contain abundant porous structures, showing increased absorption of ions and inelastic collisions. A large amount of frictional heat produced by the collisions results in an increase in tumor cell death under microwave irradiation. This can effectively inhibit tumor growth in mice by microwave ablation with good anti-tumor effects (95.4%). Remarkably, the Zn^{2+} released from the degradation of BSA@ZIF-8 enables the damage of the bacterial cell walls, and destruction of the metabolism and structure of the membrane, leading to bacterial cell death, and ultimately achieving good antibacterial properties. On the 8th day after treatment, the number of WBCs representing inflammation in the treatment group with ZIFs was restored, while the treatment group without ZIFs was 50% higher than the initial value on the 14th day. More importantly, the synthetic ZIF-8 can be biodegradable without long-term toxicity *in vivo*. The *in vivo* experiment results showed that the BSA@ZIF-8 could protect 80% of the mice from lethal challenge with tumors and accompanying infection. The as-prepared BSA@ZIF-8, therefore, is a very powerful anticancer nanohybrid using a strategy of treating tumors with microwave ablation and simultaneously inhibiting bacterial growth to overcome the current concerns of efficient cancer therapy.

Conflicts of interest

The authors declare no conflicts of interest.

Acknowledgements

The authors acknowledge financial support from the National Natural Science Foundation of China (Project No. 61671435, 81671845 and 81630053) and the Beijing Natural Science Foundation (No. 4161003).

Notes and references

1 J. Ferlay, I. Soerjomataram, R. Dikshit, S. Eser, C. Mathers, M. Rebelo, D. M. Parkin, D. Forman and F. Bray, *Int. J. Cancer*, 2015, **136**, 359–386.
2 C. Allemani, T. Matsuda, V. D. Carlo, R. Harewood, M. Matz, M. Nikšić, A. Bonaventure, M. Valkov, C. J. Johnson, J. Estève, O. J. Ogunbiyi, G. A. e Silva, W. Chen, S. Eser, G. Engholm, C. A. Stiller, A. Monnereau, R. R. Woods, O. o Visser, G. H. Lim, J. Aitken, H. K. Weir, M. P. Coleman and C. W. Group, *Lancet*, 2018, **391**, 1023–1075.
3 L. A. Torre, F. Bray, R. L. Siegel, J. Ferlay, J. Lortet-Tieulent and A. Jemal, *Ca-Cancer J. Clin.*, 2015, **65**, 87–108.
4 R. Stupp, W. P. Mason, M. J. van den Bent, M. Weller, B. Fisher, M. J. B. Taphoorn, K. Belanger, A. A. Brandes, C. Marosi, U. Bogdahn, J. Curschmann, R. C. Janzer, S. K. Ludwin, T. Gorlia, A. Allgeier, D. Lacombe, J. G. Cairncross, E. Eisenhauer, R. O. Mirimanoff, D. Van Den Weyngaert, S. Kaendler, P. Krauseneck, N. Vinolas, S. Villa, R. E. Wurm, M. H. B. Maillot, F. Spagnolli, G. Kantor, J. P. Malhaire, L. Renard, O. De Witte, L. Scandolaro, C. J. Vecht, P. Maingon, J. Lutterbach, A. Kobierska, M. Bolla, R. Souchon, C. Mitine, T. Tzuk-Shina, A. Kuten, G. Haferkamp, J. de Greve, F. Priou, J. Menten, I. Rutten, P. Clavere, A. Malmstrom, B. Jancar, E. Newlands, K. Pigott, A. Twijnstra, O. Chinot, M. Reni, A. Boiardi, M. Fabbro, M. Campone, J. Bozzino, M. Frenay, J. Gijtenbeek, A. A. Brandes, J. Y. Delattre, U. Bogdahn, U. De Paula, M. J. van den Bent, C. Hanzen, G. Pavanato, S. Schraub, R. Pfeffer, R. Soffietti, M. Weller, R. D. Kortmann, M. Taphoorn, J. L. Torrecilla, C. Marosi, W. Grisold, P. Huget, P. Forsyth, D. Fulton, S. Kirby, R. Wong, D. Fenton, B. Fisher, G. Cairncross, P. Whitlock, K. Belanger, S. Burdette-Radoux, S. Gertler, S. Saunders, K. Laing, J. Siddiqui, L. A. Martin, S. Gulavita, J. Perry, W. Mason, B. Thiessen, H. Pai, Z. Y. Alam, D. Eisenstat, W. Mingrone, S. Hofer, G. Pesce, J. Curschmann, P. Y. Dietrich, R. Stupp, R. O. Mirimanoff, P. Thum, B. Baumert, G. Ryan and E. O. R. T. C. Br, *N. Engl. J. Med.*, 2005, **352**, 987–996.
5 J. Lai, D. Lu, C. Zhang, H. Zhu, L. Gao, Y. Wang, R. Bao, Y. Zhao, B. Jia, F. Wang, Z. Yang and Z. Liu, *Biomaterials*, 2018, **158**, 1–9.
6 S. Y. Li, H. Cheng, B. R. Xie, W. X. Qiu, J. Y. Zeng, C. X. Li, S. S. Wan, L. Zhang, W. L. Liu and X. Z. Zhang, *ACS Nano*, 2017, **11**, 7006–7018.
7 L. Rao, L. L. Bu, B. Cai, J. H. Xu, A. Li, W. F. Zhang, Z. J. Sun, S. S. Guo, W. Liu, T. H. Wang and X. Z. Zhao, *Adv. Mater.*, 2016, **28**, 3460–3466.
8 Y. Ma, S. L. Qiao, Y. Wang, Y. X. Lin, H. W. An, X. C. Wu, L. Wang and H. Wang, *Biomaterials*, 2018, **156**, 248–257.
9 Q. Chen, L. Feng, J. Liu, W. Zhu, Z. Dong, Y. Wu and Z. Liu, *Adv. Mater.*, 2016, **28**, 7129–7136.
10 J. N. Liu, W. Bu and J. Shi, *Chem. Rev.*, 2017, **117**, 6160–6224.
11 J. Ge, Q. Jia, W. Liu, L. Guo, Q. Liu, M. Lan, H. Zhang, X. Meng and P. Wang, *Adv. Mater.*, 2015, **27**, 4169–4177.
12 K. F. Chu and D. E. Dupuy, *Nat. Rev. Cancer*, 2014, **14**, 199–208.
13 N. Lee, D. Yoo, D. Ling, M. H. Cho, T. Hyeon and J. Cheon, *Chem. Rev.*, 2015, **115**, 10637–10689.
14 Y. Cao, S. Li, C. Chen, D. Wang, T. Wu, H. Dong and X. Zhang, *Biomaterials*, 2018, **158**, 23–33.
15 P. Hu, T. Wu, W. Fan, L. Chen, Y. Liu, D. Ni, W. Bu and J. Shi, *Biomaterials*, 2017, **141**, 86–95.
16 Q. Xiao, X. Zheng, W. Bu, W. Ge, S. Zhang, F. Chen, H. Xing, Q. Ren, W. Fan, K. Zhao, Y. Hua and J. Shi, *J. Am. Chem. Soc.*, 2013, **135**, 13041–13048.
17 L. Rao, B. Cai, L. L. Bu, Q. Q. Liao, S. S. Guo, X. Z. Zhao, W. F. Dong and W. Liu, *ACS Nano*, 2017, **11**, 3496–3505.
18 Y. Liu, J. Zhang, C. Zuo, Z. Zhang, D. Ni, C. Zhang, J. Wang, H. Zhang, Z. Yao and W. Bu, *Nano Res.*, 2016, **9**, 3257–3266.
19 Y. Tang, T. Yang, Q. Wang, X. Lv, X. Song, H. Ke, Z. Guo, X. Huang, J. Hu, Z. Li, P. Yang, X. Yang and H. Chen, *Biomaterials*, 2018, **154**, 248–260.
20 W. Yang, J. Noh, H. Park, S. Gwon, B. Singh, C. Song and D. Lee, *Biomaterials*, 2018, **154**, 48–59.
21 M. S. Khan, A. Talib, S. Pandey, M. L. Bhaisare, G. Gedda and H. F. Wu, *Colloids Surf., B*, 2017, **159**, 564–570.
22 D. K. Macharia, Q. Tian, L. Chen, Y. Sun, N. Yu, C. He, H. Wang and Z. Chen, *J. Photochem. Photobiol., B*, 2017, **174**, 10–17.

23 J. Xu, Y. Chen, L. Deng, J. Liu, Y. Cao, P. Li, H. Ran, Y. Zheng and Z. Wang, *Biomaterials*, 2016, **106**, 264–275.
24 H. Shi, T. Liu, C. Fu, L. Li, L. Tan, J. Wang, X. Ren, J. Ren, J. Wang and X. Meng, *Biomaterials*, 2015, **44**, 91–102.
25 D. Long, M. Niu, L. Tan, C. Fu, X. Ren, K. Xu, H. Zhong, J. Wang, L. Li and X. Meng, *Nanoscale*, 2017, **9**, 8834–8847.
26 J. Mao, S. Tang, D. Hong, F. Zhao, M. Niu, X. Han, J. Qi, H. Bao, Y. Jiang, C. Fu, D. Long, X. Meng and H. Su, *Nanoscale*, 2017, **9**, 3429–3439.
27 H. Peng, B. Cui, G. Li, Y. Wang, N. Li, Z. Chang and Y. Wang, *Mater. Sci. Eng., C*, 2015, **46**, 253–263.
28 X. Duan, P. Chen, X. Han, J. Ren, Z. Wang, G. Zhao and H. Li, *Sci. Rep.*, 2017, **7**, 12677.
29 H. Kuper, H. O. Adami and D. Trichopoulos, *J. Intern. Med.*, 2000, **248**, 171–183.
30 F. Balkwill and A. Mantovani, *Lancet*, 2001, **357**, 539–545.
31 L. M. Coussens and Z. Werb, *Nature*, 2002, **420**, 860–867.
32 D. Daniel, N. Meyer-Morse, E. K. Bergsland, K. Dehne, L. M. Coussens and D. Hanahan, *J. Exp. Med.*, 2003, **197**, 1017–1028.
33 B. F. Sloane, S. Yan, I. Podgorski, B. E. Linebaugh, M. L. Cher, J. Mai, D. Cavallo-Medved, M. Sameni, J. Dosescu and K. Moin, *Semin. Cancer Biol.*, 2005, **15**, 149–157.
34 S. I. Grivennikov, F. R. Greten and M. Karin, *Cell*, 2010, **140**, 883–899.
35 M. Pesic and F. R. Greten, *Curr. Opin. Cell Biol.*, 2016, **43**, 55–61.
36 J. R. Melamed, R. S. Edelstein and E. S. Day, *ACS Nano*, 2015, **9**, 6–11.
37 Q. Dong, X. Wang, X. Hu, L. Xiao, L. Zhang, L. Song, M. Xu, Y. Zou, L. Chen, Z. Chen and W. Tan, *Angew. Chem., Int. Ed. Engl.*, 2018, **57**, 177–181.
38 Y. Liu, X. Xu, Q. Xia, G. Yuan, Q. He and Y. Cui, *Chem. Commun.*, 2010, **46**, 2608–2610.
39 J. Quirós, K. Boltes, S. Aguado, R. G. de Villoria, J. J. Vilatela and R. Rosal, *Chem. Eng. J.*, 2015, **262**, 189–197.
40 A. W. Peters, Z. Li, O. K. Farha and J. T. Hupp, *ACS Appl. Mater. Interfaces*, 2016, **8**, 20675–20681.
41 G. Lu, S. Li, Z. Guo, O. K. Farha, B. G. Hauser, X. Qi, Y. Wang, X. Wang, S. Han, X. Liu, J. S. DuChene, H. Zhang, Q. Zhang, X. Chen, J. Ma, S. C. Loo, W. D. Wei, Y. Yang, J. T. Hupp and F. Huo, *Nat. Chem.*, 2012, **4**, 310–316.
42 N. Ding, H. Li, X. Feng, Q. Wang, S. Wang, L. Ma, J. Zhou and B. Wang, *J. Am. Chem. Soc.*, 2016, **138**, 10100–10103.
43 H. Zheng, Y. Zhang, L. Liu, W. Wan, P. Guo, A. M. Nystrom and X. Zou, *J. Am. Chem. Soc.*, 2016, **138**, 962–968.
44 H. Zhang, W. Chen, K. Gong and J. Chen, *ACS Appl. Mater. Interfaces*, 2017, **9**, 31519–31525.
45 S. Li, K. Wang, Y. Shi, Y. Cui, B. Chen, B. He, W. Dai, H. Zhang, X. Wang, C. Zhong, H. Wu, Q. Yang and Q. Zhang, *Adv. Funct. Mater.*, 2016, **26**, 2715–2727.
46 J. Yu, C. Yang, J. Li, Y. Ding, L. Zhang, M. Z. Yousaf, J. Lin, R. Pang, L. Wei, L. Xu, F. Sheng, C. Li, G. Li, L. Zhao and Y. Hou, *Adv. Mater.*, 2014, **26**, 4114–4120.
47 C. Adhikari, A. Das and A. Chakraborty, *Mol. Pharmaceutics*, 2015, **12**, 3158–3166.
48 C. Y. Sun, C. Qin, C. G. Wang, Z. M. Su, S. Wang, X. L. Wang, G. S. Yang, K. Z. Shao, Y. Q. Lan and E. B. Wang, *Adv. Mater.*, 2011, **23**, 5629–5632.
49 M. Yu, D. You, J. Zhuang, S. Lin, L. Dong, S. Weng, B. Zhang, K. Cheng, W. Weng and H. Wang, *ACS Appl. Mater. Interfaces*, 2017, **9**, 19698–19705.
50 S. Lin, X. Liu, L. Tan, Z. Cui, X. Yang, K. W. K. Yeung, H. Pan and S. Wu, *ACS Appl. Mater. Interfaces*, 2017, **9**, 19248–19257.
51 G. Wyszogrodzka, B. Marszalek, B. Gil and P. Dorozynski, *Drug Discovery Today*, 2016, **21**, 1009–1018.
52 C. Tamames-Tabar, E. Imbuluzqueta, N. Guillou, C. Serre, S. R. Miller, E. Elkaïm, P. Horcajada and M. J. Blanco-Prieto, *CrystEngComm*, 2015, **17**, 456–462.
53 A. R. Chowdhuri, B. Das, A. Kumar, S. Tripathy, S. Roy and S. K. Sahu, *Nanotechnology*, 2017, **28**, 095102.
54 A. C. McKinlay, P. K. Allan, C. L. Renouf, M. J. Duncan, P. S. Wheatley, S. J. Warrender, D. Dawson, S. E. Ashbrook, B. Gil, B. Marszalek, T. Düren, J. J. Williams, C. Charrier, D. K. Mercer, S. J. Teat and R. E. Morris, *APL Mater.*, 2014, **2**, 124108.
55 P. Bhadra, M. K. Mitra, G. C. Das, R. Dey and S. Mukherjee, *Mater. Sci. Eng., C*, 2011, **31**, 929–937.
56 K. R. Raghupathi, R. T. Koodali and A. C. Manna, *Langmuir*, 2011, **27**, 4020–4028.
57 L. Zhang, Y. Ding, M. Povey and D. York, *Prog. Nat. Sci.*, 2008, **18**, 939–944.
58 T. Amna, M. S. Hassan, N. A. Barakat, D. R. Pandeya, S. T. Hong, M. S. Khil and H. Y. Kim, *Appl. Microbiol. Biotechnol.*, 2012, **93**, 743–751.
59 R. Wahab, Y. S. Kim, A. Mishra, S. I. Yun and H. S. Shin, *Nanoscale Res. Lett.*, 2010, **5**, 1675–1681.
60 J. T. Seil and T. J. Webster, *Int. J. Nanomed.*, 2008, **3**, 523–531.
61 J. P. Ruparelia, A. K. Chatterjee, S. P. Duttagupta and S. Mukherji, *Acta Biomater.*, 2008, **4**, 707–716.
62 H. Shi, M. Niu, L. Tan, T. Liu, H. Shao, C. Fu, X. Ren, T. Ma, J. Ren, L. Li, H. Liu, K. Xu, J. Wang, F. Tang and X. Meng, *Chem. Sci.*, 2015, **6**, 5016–5026.
63 D. Long, T. Liu, L. Tan, H. Shi, P. Liang, S. Tang, Q. Wu, J. Yu, J. Dou and X. Meng, *ACS Nano*, 2016, **10**, 9516–9528.
64 C. Fu, H. Zhou, L. Tan, Z. Huang, Q. Wu, X. Ren, J. Ren and X. Meng, *ACS Nano*, 2018, **12**, 2201–2210.
65 M. Di Piazza, C. S. Nowell, U. Koch, A. D. Durham and F. Radtke, *Cancer Cell*, 2012, **22**, 479–493.
66 B. Sanz, M. P. Calatayud, T. E. Torres, M. L. Fanarraga, M. R. Ibarra and G. F. Goya, *Biomaterials*, 2017, **114**, 62–70.